Received: 17 August 2016 | Revised: 30 August 2016 | Accepted: 11 September 2016

DOI 10.1002/aoc.3655

WILEY Applied Organometallic Chemistry

FULL PAPER

Dose-, time-and lipophilicity-dependent silver(I)–N-heterocyclic carbene complexes: Synthesis, characterization and interaction with plasmid and *Aedes albopictus* DNA

Patrick O. Asekunowo[1] | Rosenani A. Haque[1] | Mohd.R. Razali[1] | Silas W. Avicor[2] | Mustafa F.F. Wajidi[2]

[1] School of Chemical Sciences, Universiti Sains Malaysia, 11800 USM, Penang, Malaysia

[2] Molecular Entomology Research Group, School of Distance Education, Universiti Sains Malaysia, 11800 USM, Penang, Malaysia

Correspondence
Rosenani A. Haque, School of Chemical Sciences, Universiti Sains Malaysia, 11800 USM, Penang, Malaysia.
Email: rosenani@usm.my

Funding information
Universiti Sains Malaysia for the Research University, Grant/Award Number: 1001/PKIMIA/811346.

Four new Ag(I)–N-heterocyclic carbene (NHC) complexes (**5**–**8**) bearing symmetrically substituted NHC ligands have been synthesized starting from the corresponding benzimidazolium bromide salts which are accessible in a single step from *N*-substituted benzimidazoles (*N*-alkyl and *N*-aryl) and subsequently reacted with the basic metal source Ag_2O in acetonitrile–methanol. These compounds were characterized using elemental analyses, ^{1}H NMR, ^{13}C NMR, Fourier transform infrared and UV–visible spectroscopic techniques, and molar conductivity. Single-crystal structural studies for complex **5** show that the Ag(I) centre has a perfectly linear C–Ag–C coordination, with quasi-parallel pairs of aromatic benzimidazole planes. All the complexes interact with *Aedes albopictus* DNA via intercalation mode by a large hypochromicity of 22 and 27% and smaller hypochromicity of 16 and 19%. Furthermore, all complexes exhibit efficient DNA cleavage activity via a non-oxidative mechanistic pathway. The DNase activities of the test compounds revealed a time- and concentration-dependent activity pattern. The Ag(I)–NHC complexes showed considerably higher DNA cleavage activity compared to their respective benzimidazolium salts at a lower concentration. The DNA cleavage of these complexes changed from a moderate effect to a good one, corresponding to the increasing lipophilicity order of the complexes as **5** < **6** < **7** < **8** (1.02, 1.05, 1.78 and 2.06 for **5**–**8**, respectively). This order is further corroborated with the DNA binding study, but with the exception of complex **5**, which shows a better binding ability for DNA ($K_b = 3.367 \times 10^6$) than complexes **6**–**8** (6.982×10^5, 8.376×10^5 and 1.223×10^6, respectively).

KEYWORDS

Aedes albopictus DNA, Ag–NHC complex, DNA binding, N-heterocyclic carbene, nuclease activity, X-ray diffraction

1 | INTRODUCTION

The potential of metal complexes as therapeutic agents is a very crucial aspect of their utility. Complexes are presently being utilized in combination with spectroscopic and biological procedures to probe the interactions of DNA and its many structural forms.[1] Metal complexes have shown interesting propensity to bind DNA through a large number of interactions and to cleave double-stranded DNA, as a result of their innate chemical, electrochemical and photochemical properties. There has been much interest over the last few decades in the non-covalent interactions of transition metal complexes with DNA and RNA.[2–7] Continuous demand for new biologically active drugs has encouraged chemotherapeutic research based on the use of metals, since metal-based drugs may be less toxic and more prone to exhibit anti-proliferative activity against tumours.[8,9]

The interactions of organic and inorganic molecules, etc., with DNA can impede a number of processes such as transcription, replication and other cellular transactions.[10] By so doing various disorders like cancer, cystic fibrosis, malaria, and dengue fever can be treated by using DNA as targets for drugs. A lot of research has been directed at finding a number of bioactive metal complexes. Transition metals like silver have been used for years as antimicrobial agents. Silver has low toxicity as compared to other transition metals. Silver nitrate is still being used as a preventive drug against the development of neonatal conjunctivitis in infants. One of the most commonly used compounds of silver is silver(I) sulfazine; it is used to treat severe burns to prevent them from succumbing to bacterial infections.[11] Silver sulfadiazine is also an anti-infective metal complex against urinary tract infections.[12] Cleavage of DNA can be achieved by targeting its basic constituents like base and/or sugar by an oxidative pathway or by hydrolysis of phosphoester linkages.[8,9] On the other hand, DNA binding can occur through control of transcription factor, where the drug molecule interacts with the protein that binds to the DNA and hence altering its functions. Interactions can also occur through direct binding of molecules; here the drug molecule can directly bind to the DNA. Examples of such molecules are groove binders and intercalators.[13] We have previously reported some interesting interactions of Ag(I)–N-heterocyclic carbene (NHC) complexes with both plasmid DNA and RNA.[2–4] However, in this present study we are taking a step further in investigating their binding properties against the DNA of the major dengue vector *Aedes albopictus*.

The *A. albopictus* mosquito is an important vector of dengue, a fatal disease that lacks vaccines or drugs for preventive and curative purposes.[14] The absence of chemo-preventive and chemo-therapeutic agents restricts the control of this disease to vector-based control methods.[14] The most widespread vector control practice is insecticide-based control. However, dengue vectors have evolved resistance to insecticides due to various mechanisms,[15,16] reducing the potency of insecticide-based vector control and jeopardising efforts to halt the spread of dengue.

The purpose of the study reported here was to develop a methodology for the synthesis of new symmetrically substituted (benz)imidazolium-based Ag(I)–NHC complexes; and to further investigate their interactions with plasmid and *A. albopictus* DNA (*Aa*-DNA) as an attempt to study their potential as antibacterial and anti-dengue vector agents. The structures of these compounds were correlated with their lipophilicity in order to establish a structure–activity relationship.

2 | EXPERIMENTAL

2.1 | Materials, methods and instrumentation

All reactions were carried out under aerobic conditions. All Ag_2O reactions were carried out under the exclusion of light. The solvents were of analytical grade and used without further purification or drying. NMR spectra were recorded with a Bruker 500 MHz spectrometer at room temperature in DMSO-d_6. Chemical shifts (δ) were internally referenced to the residual solvent signals relative to tetramethylsilane. The values of chemical shifts are given in ppm and values for coupling constants (J) in Hz. Abbreviations for signal multiplicities are as follows: singlet (s), doublet (d), triplet (t), quartet (q), multiplet (m) and broad (br). FT-IR spectra were recorded with a PerkinElmer system 2000 FT-IR spectrophotometer in the range 400–4000 cm^{-1}. Elemental analyses for C, H and N were carried out with a PerkinElmer series II, 2400 microanalyzer. All electronic absorption spectra were obtained using a quartz crystal cuvette with a PerkinElmer Lambda 35 spectrometer. Emission spectra were recorded with a PerkinElmer LS 55 fluorescence spectrophotometer. Melting points were measured using a Stuart Scientific SMP-1 (UK) instrument. Conductivity measurement was conducted with a Jenway 470 conductivity/TDS meter, with conductivity resolution of 0.01 μS–1 mS and accuracy of ±0.5% ± 2 digits. Crystals were mounted on fine glass fibre or metal pin using viscous hydrocarbon oil. Data were collected with a Bruker Smart ApexII-2009 CCD diffractometer, equipped with graphite monochromated Mo Kα radiation (λ = 0.71073 Å). Data collection temperatures were maintained at 100 K using open flow N_2 cryostreams. Integration was carried out by the program SAINT using APEX II software.[17] Solutions were obtained by direct methods using SHELXS97, followed by successive refinements using full-matrix least-squares methods against F^2 using SHELXL97.[18] The program X-seed was used as graphical SHELX interface.[19] Crystal data and refinement details for complex **5** are provided in Table 1.

2.2 | Synthesis of benzimidazolium salts

2.2.1 | 1,3-Bis(benzylbenzimidazolium) hexafluorophosphate (1)

To a stirring solution of benzimidazole (1.00 g, 8.46 mmol) in 1,4-dioxane (20 ml), benzyl bromide (2.89 g, 16.90 mmol) was added. The mixture was heated at 90 °C for 24 h to obtain thick yellowish oil, which was decanted in order to remove the solvent and washed with dioxane and diethyl ether. The bromide salt obtained was converted to its hexafluorophosphate counterpart using KPF_6 (3.11 g, 16.90 mmol) in methanol (20 ml). The mixture was stirred at room temperature for 3 h and allowed to stand overnight. Then the solvent was removed under reduced pressure and the resultant beige powder was washed with distilled water (3 × 5 ml) to remove unreacted KPF_6, and air-dried to yield compound **1**. Recrystallization from acetonitrile–methanol gave the compound as a crystalline solid.

Yield 66%; m.p. 118–120 °C. ^{1}H NMR (500 MHz, DMSO-d_6, 298 K, δ, ppm): 5.80 (s, 4H, 2 × CH_2-benzyl); 7.43 (m, 6H, $CH_{\text{-benzyl}}$); 7.54 (m, 4H, $CH_{\text{-benzyl}}$); 7.67 (m, 2H, $CH_{\text{-benzimidazole}}$); 7.94 (m, 2H, $CH_{\text{-benzimidazole}}$); 10.03

TABLE 1 Crystal data and structure refinement details for complex **5**

Formula	$C_{42}H_{36}Ag\ F_6N_4P$
Formula weight	849.59
Crystal system	Triclinic
Space group	P-1
a (Å)	8.2460(4)
b (Å)	10.7905(6)
c (Å)	11.7005(6)
α (°)	69.617(3)
β (°)	86.721(3)
γ (°)	68.223(3)
V (Å^3)	903.15(9)
Z	1
ρ calcd (g cm^{-3})	1.562
Temperature (K)	100
μ (mm^{-1})	0.671
Crystal size (mm)	0.07 × 0.09 × 0.68
θ range (°)	1.9–31.6
Reflections measured	21 427
Reflections unique	5963
Reflections with $I \geq 2\ s(I)$	4657
R(int)	0.049
$R\ [I \geq 2\ s(I)]$	0.053
wR_2	0.11
S	1.05

(s,1H, NC*H*N). $^{13}C\{^1H\}$ NMR (125 MHz, DMSO-d_6, 298 K, *δ*, ppm): 52.7 (CH_2-benzyl); 114.2, 125.6, 128.1, 129.5 (C-$_{benzyl}$); 131.5, 134.3, 136.7 (C-4/7, C-5/6, C-8/9; C-$_{benzimidazole}$); 138.4 (N*C*N). FT-IR (KBr disc, cm^{-1}): *ca* 3123 (C–H_{ar}); 1450 (C═N). UV–visible (DMSO, nm): λ 279.5 (*ε* 10 177 M^{-1} cm^{-1}), λ 288 (*ε* 7846 M^{-1} cm^{-1}). Anal. Calcd for $C_{21}H_{19}N_2F_6P$ (%): C, 56.87; H, 4.35; N, 6.33. Found (%): C, 57.21; H, 4.75; N, 6.57.

2.2.2 | 1,3-Bis(hexylbenzimidazolium) hexafluorophosphate (2)

KOH (1.43 g, 25.40 mmol) was added to a stirring solution of benzimidazole (2.00 g, 16.93 mmol) in DMSO (30 ml). The mixture was stirred for 1 h at room temperature and 1-bromohexane (2.79 g, 16.93 mmol) was added dropwise. After 2 h the mixture was poured into 200–300 ml of water and extracted with chloroform (3 × 30 ml). The extract was filtered thrice through four plies of Whatman filter papers in order to dry the extract. The desired compound was finally evaporated under reduced pressure and was obtained as thick colourless oil. The compound formed, *N*-hexylbenzimidazole (1.00 g, 4.90 mmol), was added dropwise in a stirring solution of bromohexane (0.81 g, 4.90 mmol) in acetonitrile (30 ml) and refluxed for 20 h. The solvent was removed under reduced pressure to give 1,3-bis(hexylbenzimidazolium) bromide which was then reacted with a solution of KPF_6 (1.equiv.) in methanol (20 ml). The mixture was stirred at room temperature for 3 h and allowed to stand overnight. Then the solvent was removed under reduced pressure and the resultant white powder was washed with distilled water (3 × 5 ml) to remove unreacted KPF_6, and air dried. The powder was recrystallized from a solution of acetonitrile–methanol to obtain a crystalline solid.

Yield 61%; m.p. 134–136 °C. ^1H NMR (500 MHz, DMSO-d_6, 298 K, *δ*, ppm): 0.85 (t, *J* = 7.0 Hz, 6H, 2 × CH_3); 1.25 (m, 4H, 2 × CH_2—CH_3); 1.33 (m, 8H, 2 × CH_2—CH_2—CH_2-CH_3); 1.89 (m, 4H, 2 × N-CH_2-CH_2); 4.52 (t, *J* = 7.0 Hz, 4H, 2 × N—CH_2—R); 7.66 (m, 2H C5/6-H-$_{benzimidazole}$); 8.07 (m, 2H C4/7-H-$_{benzimidazole}$); 9.91 (s, 1H, NC*H*N). $^{13}C\{1H\}$ NMR (125 MHz, DMSO-d_6, 298 K, *δ*, ppm): 14.5 (CH_3); 21.9 (CH_2); 25.9 (CH_2); 28.3 (CH_2); 30.3 (CH_2); 46.5 (N—CH_2); 114.5, 127.1, 131.4 (C-4/7, C-5/6, C-8/9; C-$_{benzimiazole}$); 138.5 (N*C*N). FT-IR (KBr disc, cm^{-1}): *ca* 3067 (C—H_{ar}); 2967 (C—H_{aliph}); 1471 (C═N). UV–visible (DMSO, nm): λ 279.5 (*ε* 8928 M^{-1} cm^{-1}), λ 288.5 (*ε* 6822 M^{-1} cm^{-1}). Anal. Calcd for $C_{19}H_{31}N_2F_6P$ (%): C, 52.78; H, 7.18; N, 6.48. Found (%): C, 52.92; H, 7.38; N, 6.75.

2.2.3 | 1,3-Bis(heptylbenzimidazolium) bromide (3)

Salt **3** was prepared analogously to **2** using *N*-heptylbenzimidazole (1.00 g, 3.34 mmol) and 1-bromoheptane (0.78 g, 4.34 mmol) in acetonitrile (20 ml) to produce **3** as a white solid.

Yield 62%; m.p. 145–147 °C. ^1H NMR (500 MHz, DMSO-d_6, 298 K, *δ*, ppm): 0.81 (t, *J* = 7.0 Hz, 6H, 2 × CH_3); 1.19 (m, 4H, 2 × CH_2—CH_3); 1.33 (m, 12H, 2 × CH_2—CH_2—CH_2—CH_3); 1.92 (m, 4H, 2 × N—CH_2—CH_2); 4.52 (t, *J* = 7.0 Hz, 4H, 2 × N—CH_2—R); 7.69 (m, 2H C5/6-H-$_{benzimidazole}$); 8.12 (m, 2H C4/7-H-$_{benzimidazole}$); 9.99 (s, 1H, NC*H*N). $^{13}C\{1H\}$ NMR (125 MHz, DMSO-d_6, 298 K, *δ*, ppm): 14.5 (CH_3); 21.9 (CH_2); 25.9 (CH_2); 27.3 (CH_2); 30.3 (CH_2); 31.7 (CH_2); 48.5 (N—CH_2); 114.5, 127.1, 131.4 (C-4/7, C-5/6, C-8/9; C-$_{benzimiazole}$); 138.5 (N*C*N). FT-IR (KBr disc, cm^{-1}): *ca* 3077 (C—H_{ar}); 2972 (C—H_{aliph}); 1470 (C═N). UV–visible (DMSO, nm): λ 279 (*ε* 9928 M^{-1} cm^{-1}), λ 287 (*ε* 7479 M^{-1} cm^{-1}). Anal. Calcd for $C_{21}H_{35}N_2Br$ (%): C, 63.80; H, 8.86; N, 7.09. Found (%): C, 63.92; H, 9.04; N, 7.15.

2.2.4 | 1,3-Bis(octylbenzimidazolium) bromide (4)

Salt **4** was prepared analogously to **2** using *N*-octylbenzimidazole (1.00 g, 3.87 mmol) and 1-bromooctane (0.75 g, 3.87 mmol) in acetonitrile (20 ml) to produce **4** as a white solid.

Yield 57%; m.p. 150–152 °C. ^1H NMR (500 MHz, DMSO-d_6, 298 K, *δ*, ppm): 0.84 (t, *J* = 7.0 Hz, 6H, CH_3); 1.27 (m, 4H, 2 × CH_2—CH_3); 1.36 (m, 16H, 2 × N—CH_2—CH_2—CH_2—CH_2—CH_2—CH_2—); 1.95 (m, 4H, 2 × N—CH_2—CH_2); 4.58 (t, *J* = 7.0 Hz, 4H, 2 × N—CH_2—R); 7.72 (m, 2H C5/6-H-$_{benzimidazole}$); 8.12

(m, 2H C4/7-H-$_{benzimidazole}$); 10.07 (s, 1H, NC*H*N). ^{13}C {1H} NMR (125 MHz, DMSO-d_6, 298 K, δ, ppm): 14.5 (CH_3); 21.9 (CH_2); 23.4 (CH_2); 25.9 (CH_2); 27.3 (CH_2); 30.3 (CH_2); 31.7 (CH_2); 48.5 (N-CH_2); 118.5, 129.4, 131.8 (C-4/7, C-5/6, C-8/9; C-$_{benzimiazole}$); 142.5 (N*C*N). FT-IR (KBr disc, cm^{-1}): *ca* 3037 (C—H_{ar}); 2962 (C—H_{aliph}); 1479 (C=N). UV–visible (DMSO, nm): λ 279.5 (ε 10 065 M^{-1} cm^{-1}), λ 288 (ε 7677 M^{-1} cm^{-1}). Anal. Calcd for $C_{23}H_{39}N_2Br$ (%): C, 65.25; H, 9.22; N, 6.62. Found (%): C, 65.42; H, 9.44; N, 6.77.

2.3 | Synthesis of Ag(I)–NHC complexes

2.3.1 | 1,3-Bis(benzylbenzimidazolium)silver(I) hexafluorophosphate (5)

To a suspension of **1** (0.50 g, 1.00 mmol) in acetonitrile (40 ml) was added Ag_2O (0.24 g, 1.00 mmol). The mixture was stirred at 50–60 °C for 12 h under the exclusion of light. The obtained brown solution was filtered through a pad of celite and the filtrate was slowly evaporated to precipitate a pale brown solid. The compound was further purified by acetonitrile–dichloromethane to give a crystalline solid. Single crystals suitable for X-ray analysis were obtained by the slow diffusion of diethyl ether into acetonitrile solution containing the complex.

Yield 70%; m.p. 220–222 °C. ^{1}H NMR (500 MHz, DMSO-d_6, 298 K, δ, ppm): 5.80 (s, 8H, 4 × CH_2-benzyl); 7.25–7.40 (m, 12H, CH-$_{benzyl}$); 7.45–7.54 (m, 8H, CH-$_{benzyl}$); 7.77 (m, 2H, CH-$_{benzimidazole}$); 7.90 (m, 2H, CH-$_{benzimidazole}$). ^{13}C{^{1}H} NMR (125 MHz, DMSO-d_6, 298 K, δ, ppm): 52.7 (CH_2-benzyl); 114.2, 125.6, 128.1, 129.5 (C-$_{benzyl}$); 131.5, 134.3, 136.7 (C-4/7, C-5/6, C-8/9; C-$_{benzimidazole}$). FT-IR (KBr disc, cm^{-1}): *ca* 3105 ν (C—H_{ar}); 2977 (C—H_{aliph}); 1290 (C—N). UV–visible (DMSO, nm): λ 277 (ε 15 097 M^{-1} cm^{-1}), λ 284.5 (ε 9829 M^{-1} cm^{-1}). Anal. Calcd for $C_{42}H_{36}N_4AgF_6P$ (%): C, 59.32; H, 4.24; N, 6.59. Found (%): C, 59.48; H, 4.42; N, 6.82.

2.3.2 | 1,3-Bis(hexylbenzimidazolium)silver(I) hexafluorophosphate (6)

Complex **6** was prepared in the same way as **5**, except that **1** was replaced with **2** (1.50 g, 3.50 mmol) and Ag_2O (0.81 g, 3.50 mmol). Complex **6** was isolated as pale brown powder.

Yield 62%; m.p. 231–233 °C. ^{1}H NMR (500 MHz, DMSO-d_6, 298 K, δ, ppm): 0.73 (t, J = 7.0 Hz, 12H, 4 × CH_3); 1.11 (m, 8H, 4 × *CH_2*—CH_3); 1.25 (m, 16H, 4 × *CH_2*—*CH_2*—CH_2—CH_3); 1.90 (m, 8H, 4 × N—CH_2—*CH_2*); 4.60 (t, J = 7.0 Hz, 8H, 4 × N—CH_2—R); 7.50 (m, 4H C5/6-H-$_{benzimidazole}$); 7.85 (m, 4H C4/7-H-$_{benzimidazole}$). ^{13}C{1H} NMR (125 MHz, DMSO-d_6, 298 K, δ, ppm): 12.5 (CH_3); 20.4 (CH_2); 25.9 (CH_2); 28.3 (CH_2); 30.3 (CH_2); 46.5 (N—CH_2); 114.5, 127.1, 131.4 (C-4/7, C-5/6, C-8/9; C-$_{benzimiazole}$); 187.5 (C2—Ag). FT-IR (KBr disc, cm^{-1}): *ca* 3060 (C—H_{ar}); 2959 (C—H_{aliph}); 1462 (C=N). UV–visible (DMSO, nm): λ 277.5 (ε 11 928 M^{-1} cm^{-1}), λ 288.5 (ε 8822 M^{-1} cm^{-1}). Anal. Calcd for $C_{38}H_{60}N_4AgF_6P$ (%): C, 55.27; H, 7.27; N, 6.79. Found (%): C, 55.42; H, 7.38; N, 6.95.

2.3.3 | 1,3-Bis(heptylbenzimidazolium)silver(I) hexafluorophosphate (7)

A mixture of **3** (0.60 g, 1.96 mmol) and Ag_2O (0.75 g, 3.24 mmol) in dichloromethane (40 ml) was stirred at room temperature for 24 h. The reaction mixture was filtered through celite to remove unreacted silver and the solvent was removed under reduced pressure, which was then reacted with a solution of KPF_6 (1 equiv.) in methanol (20 ml). The mixture was stirred at room temperature for 3 h and allowed to stand overnight. Then the solvent was removed under reduced pressure and the resultant white powder was washed with distilled water (3 × 5 ml) to remove unreacted KPF_6, and air dried. The compound was further purified by acetonitrile–dichloromethane to give a crystalline solid.

Yield 57%; m.p. 245–247 °C. ^{1}H NMR (500 MHz, DMSO-d_6, 298 K, δ, ppm): 0.76 (t, J = 7.0 Hz, 12H, 4 × CH_3); 1.22 (m, 8H, 4 × *CH_2*—CH_3); 1.35 (m, 24H, 4 × *CH_2*—*CH_2*—*CH_2*—CH_3); 1.92 (m, 8H, 4 × N—CH_2—*CH_2*); 4.58 (t, J = 7.0 Hz, 8H, 4 × N—CH_2—R); 7.50 (m, 4H C5/6-H-$_{benzimidazole}$); 7.88 (m, 4H C4/7-H-$_{benzimidazole}$). ^{13}C {1H} NMR (125 MHz, DMSO-d_6, 298 K, δ, ppm): 12.5 (CH_3); 21.9 (CH_2); 25.9 (CH_2); 27.3 (CH_2); 30.3 (CH_2); 31.7 (CH_2); 48.5 (N—CH_2); 114.5, 127.1, 131.4 (C-4/7, C-5/6, C-8/9; C-$_{benzimiazole}$); 187.0, 188.5 ((d, ^1J ($_{C—109Ag}$) = 207.5 Hz; and d, ^1J($_{C—107Ag}$) = 182.0 Hz). FT-IR (KBr disc, cm^{-1}): *ca* 3047 (C—H_{ar}); 2969 (C—H_{aliph}); 1450 (C=N). UV–visible (DMSO, nm): λ 277 (ε 12 768 M^{-1} cm^{-1}), λ 284 (ε 9975 M^{-1} cm^{-1}). Anal. Calcd for $C_{42}H_{68}N_4AgF_6P$ (%): C, 57.21; H, 7.72; N, 6.36. Found (%): C, 57.33; H, 7.94; N, 6.57.

2.3.4 | 1,3-Bis(octylbenzimidazolium)silver(I) hexafluorophosphate (8)

Complex **8** was prepared in the same way as **7**, except that **3** was replaced with **4** (1.23 g, 2.90 mmol) and Ag_2O (0.67 g, 2.90 mmol). Complex **8** was isolated as a pale brown powder.

Yield 60%; m.p. 251–253 °C. ^{1}H NMR (500 MHz, DMSO-d_6, 298 K, δ, ppm): 0.73 (t, J = 7.0 Hz, 12H, 4 × CH_3); 1.14 (m, 8H, 4 × *CH_2*—CH_3); 1.30 (m, 32H, 4 × N—CH_2—CH_2—*CH_2*—*CH_2*—*CH_2*—*CH_2*—); 1.92 (m, 8H, 4 × N—CH_2—*CH_2*); 4.58 (t, J = 7.0 Hz, 8H, 4 × N—CH_2—R); 7.72 (m, 4H C5/6-H-$_{benzimidazole}$); 7.91 (m, 4H C4/7-H-$_{benzimidazole}$). ^{13}C{1H} NMR (125 MHz, DMSO-d_6, 298 K, δ, ppm): 14.5 (CH_3); 21.9 (CH_2); 23.4 (CH_2); 25.9 (CH_2); 27.3 (CH_2); 30.3 (CH_2); 31.7 (CH_2); 48.5 (N—CH_2); 118.5, 129.4, 131.8 (C-4/7, C-5/6, C-8/9; C-$_{benzimiazole}$); 188.5 (C2—Ag). FT-IR (KBr disc, cm^{-1}): *ca* 3037 (C—H_{ar}); 2962 (C—H_{aliph}); 1460 (C=N). UV–visible (DMSO, nm): λ 277.5 (ε 13 987 M^{-1} cm^{-1}), λ 284 (ε 10 127 M^{-1} cm^{-1}). Anal. Calcd for $C_{46}H_{76}N_4AgF_6P$ (%): C, 58.91; H, 8.11; N, 5.98. Found (%): C, 59.25; H, 8.44; N, 6.27.

2.4 | Stability assay

In order to assess the stability of the complexes, 10 μg ml^{-1} solutions of **5–8** in DMSO were prepared and added in a 1:1 ratio to *Aa*-DNA stock solution prepared in DMSO. This was done to imitate the conditions of the DNA evaluation experiments. The complexes used for the testing were dissolved in the minimal amount of DMSO possible and diluted with *Aa*-DNA stock solution of 10^{-6} M and less than 0.8% DMSO. UV–visible spectra were measured after 0, 24, 48 and 72 h for determining the stability of the complexes.

2.5 | Biological activity

2.5.1 | Lipophilicity assay

The experimental lipophilicity measurement (with slight modification)[20] involved partitioning of a compound between octanol and aqueous solution. Log *P* was calculated as the decimal logarithm of the ratio of the solute concentration in *n*-octanol and in water after partition equilibrium. Amounts of 20 ml of octanol, 30 ml of distilled water and 10 ml of complex were introduced into a 250 ml separating funnel. It was stirred in a mechanical shaker for 30 mins. The solutions were then left to stand for 24 h until the two phases were separated. After standing, 3 ml of solvent was extracted from the two phases then the concentrations of the compounds were determined using UV–visible spectroscopy.

Spectrophotometric UV–visible log *P determinations.* One working wavelength corresponding to the maximum of molar absorptivity was selected for each compound. In each case, the sample concentration was determined by the calibration curve constructed with four known concentrations in distilled water and *n*-octanol phases. A straight line was obtained according to the equation $y = mx + c$, where x is the concentration of the solute (mol l^{-1}) and y the absorbance at the wavelength of absorbance maximum. The linear analysis of the standard curve is shown in Figure S1 (supporting information).

2.5.2 | DNA binding assay

Mosquito strain and Aa*-DNA extraction.* Larvae of a reference *A. albopictus* strain obtained from the Vector Control Research Unit (VCRU) of Universiti Sains Malaysia were reared on larval feed consisting of Friskies® cat biscuits, beef liver, yeast and milk powder in a 2:1:1:1 ratio[21] at ambient conditions of 28 ± 3 °C and 75 ± 10% relative humidity. Emerged adults were fed on 10% sucrose solution and *Aa*-DNA was extracted from virgin individual adult females (3 days old) for DNA binding activity using DNeasy® Blood and Tissue Kit (Qiagen®) according to the manufacturer's instruction. DNA extracted from individual female mosquitoes was pooled and used for the binding study.

DNA binding analysis using electronic spectral method. The *Aa*-DNA was dissolved in buffer solution (10 mM phosphate buffer, 50 mM NaCl, pH = 7.4) as a stock solution, which was stored at 4 °C for 24 h to reach homogeneous phase and used within three days. The *Aa*-DNA concentrations were determined by spectroscopy using the following extinction coefficients at 260 nm: DNA: 6600 M^{-1} cm^{-1} (per nucleotide), 13 100 M^{-1} cm^{-1} (per base pair).[22]

In order to check its purity, the UV absorbance of *Aa*-DNA in the buffer medium was measured at 260 and 280 nm and it was found that the DNA was convincingly free from protein. The DNA binding properties of compounds **5**, **6**, **7** and **8** with *Aa*-DNA were investigated using UV–visible spectra. The complex was dissolved in DMSO to obtain the desired concentration. Absorption titration experiments were done by varying the concentration of *Aa*-DNA, while the complex concentration is kept constant (10 μM). An increasing amount of *Aa*-DNA (10 μl each time) was gradually added to the complex in buffer after it had been incubated for about 2 h at 25 °C. The UV–visible spectra were recorded after equilibration for about 5 mins. The intrinsic equilibrium DNA binding constants (K_b) along with binding site sizes (s) of the complexes to *Aa*-DNA were determined by monitoring the change of the absorption intensity of the spectral bands with increasing concentration of *Aa*-DNA. The data were then fitted to the following equations to obtain the value of K_b:[23]

$$\frac{\varepsilon_a-\varepsilon_f}{\varepsilon_b-\varepsilon_f}=\frac{\left(b-\left(b^2-2K_b^2Ct[\mathrm{DNA}]/s\right)\right)^{1/2}}{2K_bCt} \quad (1)$$

$$b=1+K_bCt+\frac{K_b[\mathrm{DNA}]}{2s} \quad (2)$$

where Ct is the constant total concentration of metal complexes, [DNA] is the total concentration of added DNA as M base pairs, ε_a is the apparent absorption in the presence of DNA, ε_f is the extinction coefficient of free Ag(I) complex in the buffer and ε_b is the extinction coefficient of the DNA-bound Ag(I)–NHC complex. The value of ε_f was obtained from a Beer's plot of the Ag(I)–NHC complex while the value of ε_b was obtained from the absorbance of a saturated Ag–DNA sample divided by the concentration Ct. The nonlinear analysis was done using origin lab version.

2.5.3 | Fluorescence titration

Fluorescence titration experiments were carried out at room temperature under the same buffer conditions as the absorption titrations. Titrations were carried out by placing the receptor (Ag–NHC complex solution) into a 3.5 ml cuvette and adding increasing amounts of [*Aa*-DNA] (0–200 μM) solution in DMSO. After each addition solutions were

allowed to equilibrate at room temperature for about 10–15 min before measurements. The fluorescence spectra of the solutions were recorded in the range 300–450 nm at an excitation wavelength of 295 nm. The quenching ability of the *Aa*-DNA was evaluated using the following equation:[24]

$$\frac{F_0}{F} = 1 + K_{SV}r$$

where F_0 and F are the fluorescence intensities in the absence and presence of the quencher, respectively, *K*sv is the linear Stern–Volmer quenching constant and r is the concentration of the quencher. *K*sv is the slope of a plot of F_0/F versus r. The analysis of the data was carried out using origin.

2.5.4 | Viscometry

Viscosity measurements were performed using an Oswald viscometer immersed in a thermostatic water bath, maintained at constant temperature (29 ± 0.1 °C). DNA concentration was kept constant in all samples, while the complex concentration was increased each time, prepared from a stock solution of 2.5 mM. Mixing of the solution was performed by bubbling nitrogen gas through the viscometer in order to aid mixing. A digital stopwatch was used for the measurement of the downward flow of the solution. This was done in triplicate for each sample in order to obtain the mean flow time. Data were plotted as viscosity $(\eta/\eta_0)^{1/3}$ versus the ratio of complex to DNA (binding ratio). The following equation was employed in the calculation of the ratio $(\eta/\eta_0)^{1/3}$:

$$\eta = \frac{t_f - t_0}{t_0} \quad (3)$$

where η is the viscosity of DNA in the presence of the complex, t_f is the experimental flow time in seconds, t_0 is the flow time of buffer in seconds and η_0 is the viscosity of DNA solution.[25,26]

2.5.5 | Gel electrophoresis

Plasmid (pDsRed-Express) extraction was conducted using the High Speed Plasmid Mini Kit (Geneaid®) according to the manufacturer's instruction. This was assayed with four concentrations (200, 100, 50 and 25 μg ml^{-1}) of the test compounds to determine their nuclease activity on plasmid DNA.

DNA cleavage/degradation activity. The cleavage/degradation assay consisted of 1 μl of the test salt/complex in a solution consisting of 5 μl of 50 mM Tris–HCl (pH = 8.0) and 4 μl of plasmid DNA (15 μg). The mixture was incubated at 37 °C for 8 and 24 h. After incubation, 5 μl of the product was electrophoresed on 0.8% agarose gel in 0.5× Tris–acetate–EDTA (TAE) buffer at 70 V for 1 h. The gel was stained in ethidium bromide (0.5 μg ml^{-1}) for 15 min and viewed under UV light in a UVP Gel-Doc-It Imaging System (Kinematics®). The nucleating ability of the synthesized benzimidazolium salts/Ag–NHC complexes was determined by their efficiency in cleaving/degrading the plasmid DNA.

3 | RESULTS AND DISCUSSION

3.1 | Synthesis

A series of symmetrically substituted benzimidazolium salts and their Ag(I)–NHC complexes was synthesized and well characterized. All the salts are synthesized via a stepwise *N*-alkylation reaction of the benzimidazole with the appropriate aryl/alkyl substituents. The stepwise reactions of benzyl bromide and bromoalkane with 1 equiv. of benzimidazole give the mono benzimidazolium bromide salts. Salt **1**, which is analogous to the previously reported salt bearing the tetrafluoroborate counterion,[27] was prepared by the reaction of benzyl bromide (2 equiv.) and benzimidazole (1 equiv.), in 1,4-dioxane. The reaction was heated at 90 °C for 24 h to obtain thick yellowish oil which was decanted in order to remove the solvent and washed with dioxane and diethyl ether. Salts **2**–**4** were prepared from benzimidazole by stepwise alkylation with the appropriate alkyl bromide in the presence of KOH in DMSO at room temperature for 2 h. The reactants were subsequently converted into their respective quaternary salts by the reaction of *N*-alkylbenzimidazole with bromohexane/heptane/octane in acetonitrile at refluxing conditions for 20–24 h. Hexafluorophosphate salts of **1** and **2** were found to be considerably more stable than the corresponding bromide salts (due to the formation of dark viscous salts) in common organic solvents such as acetonitrile and acetone and in the solid form at room temperature. Therefore the bromide salts were converted into their hexafluorophosphate counterparts by the salt metathesis reaction using KPF_6 in methanol and were obtained conveniently in powder forms. Salts **3** and **4** exhibited considerable stability and were left as bromide salts. The synthetic route for the symmetrically substituted benzimidazolium salts is shown in Scheme 1. In the first approach, respective Ag(I)–NHC complexes **5** and **6** were synthesized using a modified protocol of Wang et al. by reacting a slight excess of Ag_2O with salts **1** and **2** in acetonitrile at 50 °C for 12 h under exclusion of light (Scheme 2).[28] In the second approach, benzimidazolium bromide salts **3** and **4** reacted with Ag_2O in methanol at room temperature for 24 h. These complexes were further purified by salt metathesis in methanol using KPF_6 at room temperature to obtain the corresponding Ag(I)–NHC complexes **7** and **8** (Scheme 3). Complexes **5**–**8** were obtained in overall yields of 62–77%.

All the reported complexes were quite soluble in common organic solvents (dichloromethane, acetonitrile and DMSO), slightly soluble in water and insoluble in hexane and benzene. The prepared complexes showed good stability to moisture but were light sensitive. The prepared complexes dissolved in DMSO-d_6 monitored using ^{1}H NMR spectroscopy over a period of 7 days showed no significant changes and were stable in the biological medium over the period of the testing time as the UV–visible spectra remain unchanged in 72 h (Figure 1).

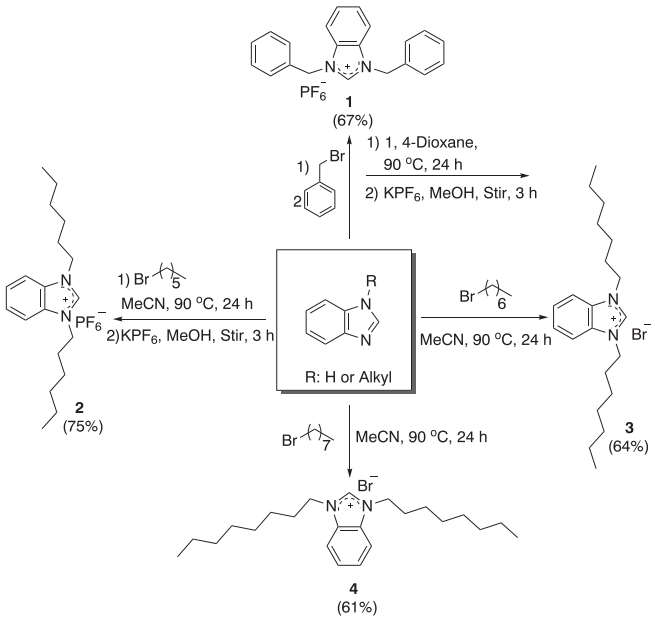

SCHEME 1 Preparation of symmetrically substituted benzimidazolium salts **1–4**

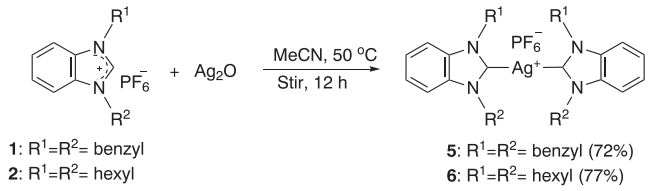

SCHEME 2 Synthetic route to Ag(I)–NHC complexes **5** and **6** from benzimidazolium salts **1** and **2**

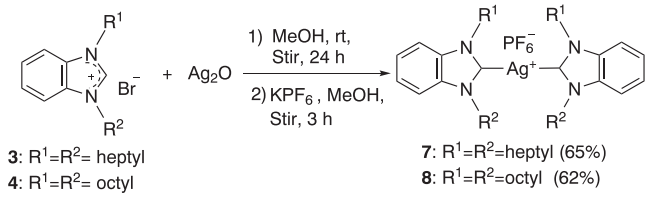

SCHEME 3 Synthetic route to Ag(I)–NHC complexes **7** and **8** from benzimidazolium salts **3** and **4**

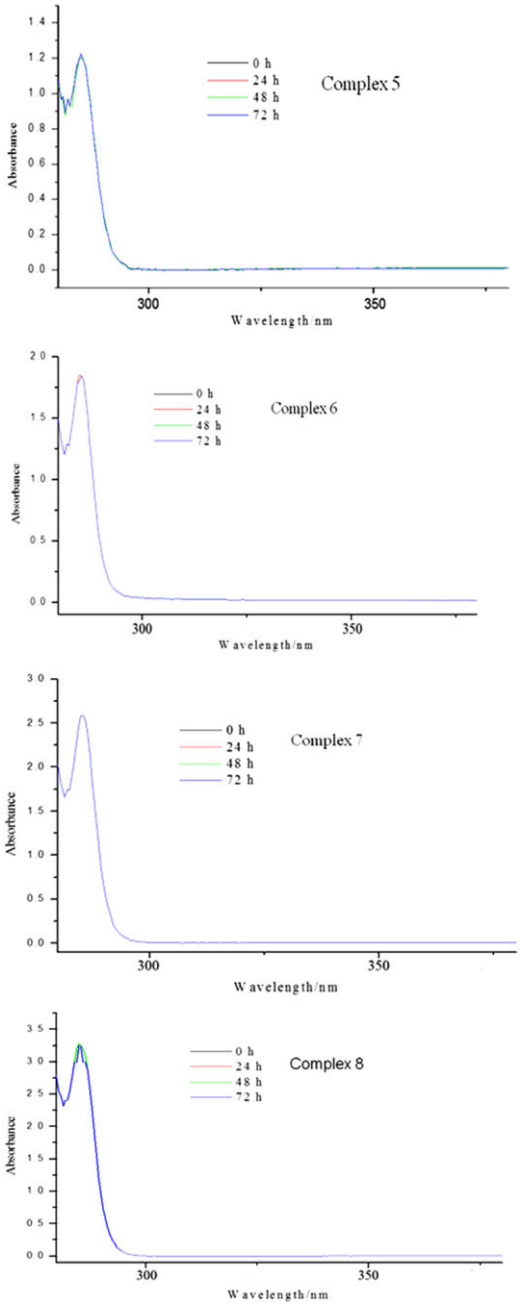

FIGURE 1 Stability of complexes **5–8** in Aa-DNA solution shown by UV-visible spectra at 0 h, 24 h, 48 h and 72 h [Absorbance vs Wavelength/nm]

3.2 | Spectroscopic characterization

The FT-IR spectra for salts **1–4** show the C─H stretching vibrational bands for the alkyl benzimidazolium salts at around 2945–3170 cm^{-1}. A band of medium intensity in the range 1475–1557 cm^{-1} is assigned to benzimidazole ring (C═N) vibrations. These vibrations show a negative shift in the Ag–NHC complex spectra (1406–1437 cm^{-1}). This shift is due to the presence of the electropositive metal centre, which affects the C─N and C═N bond vibrations by pulling electron density towards itself. Further, the FT-IR spectra of all reported compounds display two sharp bands of medium intensities in the ranges 2857–2951 and 2955–3119 cm^{-1}, assigned to aliphatic and aromatic C─H.

The ^{1}H NMR spectra of benzimidazolium salts **1–4** in DMSO-d_6 exhibit a characteristic NC*H*N proton resonance at 9.91–10.07 ppm, suggesting the successful formation of the desired salts.[16,30,31] The ^{1}H NMR spectra for the salts show similar patterns in the aromatic area in the range 7.43–8.12 ppm, which are attributed to benzene and benzimidazole rings. In the ^{13}C NMR spectra, chemical shift values of C-2 carbon are observed in the range 138.4–142.5 ppm, which is in agreement with reported data for similar benzimidazolium salts.[29–31]

In the ^{1}H NMR spectra for complexes **5–8**, the absence of resonances for the benzimidazolium carbene protons (NC*H*N) suggests the formation of the Ag(I)–NHC

complexes. This is further confirmed by the downfield shift of carbene carbon nuclei in the range 182.0–188.5 ppm for complexes **6** and **8** in the ^{13}C NMR spectra. In the case of complex **7**, the ^{13}C NMR spectrum displays resonances for the C2-carbon nuclei as two doublets centred at 187.0 and 188.5 ppm. This is due to the presence of ^{13}C–^{109}Ag and ^{13}C–^{107}Ag with the coupling constants of $^{1}J_{C—109Ag} = 205$ and $^{1}J_{C—107Ag} = 182.0$ Hz. This observation is in accord with similar reported compounds.[32,33] Surprisingly for complex **5**, the resonance for Ag–carbene carbon is not detected, despite several attempts of obtaining the ^{13}C NMR spectrum of the sample, varying the concentration and scan time. The reason was suggested in the literature as a fluxional behaviour of the NHC complexes.[34–37] The formation of this complex is, however, confirmed by X-ray data. The resonances of aromatic benzylic and aliphatic protons are observed with negligible changes when compared with the corresponding salts.

The electronic spectra of salts and complexes were recorded in DMSO solution (10^{-3} M concentration) over the range 200–400 nm. Extinction coefficients were determined from a minimum of four concentrations per sample, and were calculated by a linear regression fit of the absorbance versus concentration data. In the electronic spectra of the benzimidazolium salts, there are two typical absorption bands in the ranges 277–280 and 284–286.5 nm assigned to overlapping π–π* and n–π* transitions arising from C═C and C═N.[38] These transitions are also observed in the spectra of the complexes but are shifted to a higher energy as a result of complexation with Ag(I), indicating the formation of a C—N module in the benzimidazole ring. This confirms the coordination of the ligand to Ag(I) ion which decreases the delocalization of π electrons and as a result increases the energy of the π–π* transition. However, no bands at lower energy level for d–d transition are detected in the UV–visible region. An overlay of the electronic spectra for the four complexes (showing that they are similar but not identical) at 298 K in 10 mM phosphate buffer at pH = 7 is shown in Figure 2. Under the conditions of the DNA binding experiments at pH = 7, the spectra of all the Ag(I)–NHC complexes are basically the same as spectra recorded at pH = 10–13 and this is indicative of the fact that the complexes are not protonated.

3.3 | Molar conductivity measurements

The molar conductance values of the benzimidazolium salts and complexes were obtained at room temperature in DMF solution at 10^{-3} M concentration. The compounds were dissolved in DMF and the molar conductivities of their solutions at 25 ± 2 °C were measured The molar conductivity values of the benzimidazolium salts are found to be close, at around 23.5–26.5 S cm^2 mol^{-1}, while the values for the complexes are found to be in the range 26.6–29.9 S cm^2 mol^{-1}, indicating the ionic nature of these compounds, which are found to be 1:1 electrolytes.[39]

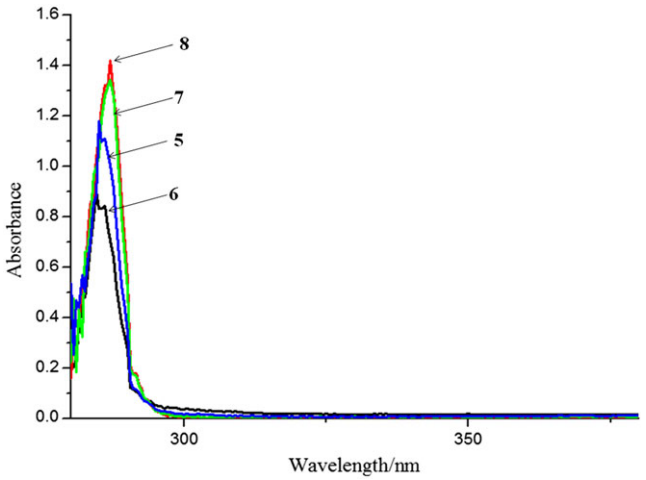

FIGURE 2 Overlay of absorption spectra of the four Ag–NHC complexes (**5**–**8**) studied in this work

Based on the foregoing, we could also deduce the structure of the compounds on the basis of their molar conductance. It is obvious from this study that each mononuclear Ag(I)–NHC complex has one hexafluorophosphate counterion to balance the Ag^+ and as a consequence reflects the formation of a mononuclear Ag–NHC complex. The molar conductivity data, elemental analysis and spectroscopy data show an agreement with the proposed structure of the compounds, which is further confirmed by means of the data obtained by single-crystal X-ray diffraction.

3.4 | Single-crystal X-ray diffraction study

Single crystals of **5** suitable for X-ray diffraction analysis were obtained from slow diffusion of diethyl ether into a solution of **5** in acetonitrile at ambient temperature, forming a colourless block. Complex **5** crystallizes in the triclinic space group *P*-1 with half of the molecule in the symmetric unit (Figure 3). The central Ag(I) is coordinated to two carbene carbon atoms, making a linear C1—Ag1—$C1^i$ bond with a bond angle of 180.0°. This observation deviates from that of a previously reported similar compound,[27] bearing the tetrafluoroborate counterion (BF_4^-), where the C—Ag—C angle was 177.88°. The dihedral angle between the planes of phenyl rings, available on the two benzimidazole moieties, is almost 90° in contrast to the tetrafluoroborate counterparts, which are 88.28° and 81.31°.

The bond distance of Ag1 with C1 (and its symmetry equivalent, $C1^i$) is 2.077(2) Å (Table 2), while the bond distance for tetrafluoroborate counterpart is 2.089 Å. The internal ring angle at the carbene centre (N1–C1–N2) is 106.6(2)°, which agrees well with reported complexes.[15,41] The π–π interactions with a separation of 3.826(5) Å are observed between two adjacent complexes, resulting in the formation of a two-dimensional supramolecular structure. In the

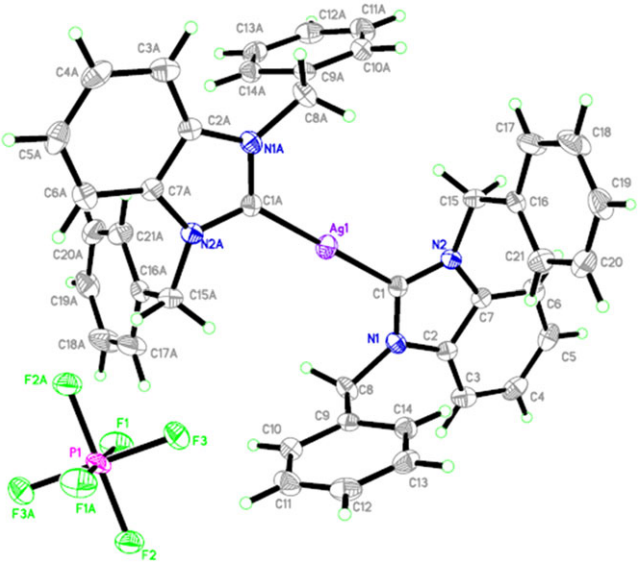

FIGURE 3 Structure of **5** with ellipsoids shown at 50% occupancies

TABLE 2 Selected bond lengths (Å) and angles (°) for **5**

Ag1–C1	2.077(2)
C1–N1	1.355(3)
C1–N2	1.353(3)
C1–Ag1–C1^{i}	180.0
Ag1–C1–N1	126.8(2)
Ag1–C1–N2	127.0(2)
N1–C1–N2	106.6(2)

extended structure, complex **5** is connected via C—H···F and C—H···N hydrogen bonds (Table 3) forming a three-dimensional network. Each fluoride ion is connected with eight different hydrogen atoms to form the hydrogen bonds.

3.5 | Lipophilicity

The lipophilicity (log *P*) is perhaps the most important physicochemical property of a potential drug. It is generally related to solubility, absorption, plasma protein binding membrane permeability and biological activities of many compounds.[42] Therefore, complexes **5**–**8** were designed with different substituents placed on the NHC groups. The complexes were tuned using different side-chain groups to explore their best lipophilicity. The lipophilicity of the complexes was determined by measuring the concentration ratio of each complex in octanol and distilled water at an equilibrium state, as summarized in Table 4. Complex **8** having the longest side chain presents the best lipophilicity of 2.06, while the lipophilicity of the complexes improves as the length of the side chain increases (**6** < **7** < **8**). Complexes **5** and **6** show similar lipophilicity of 1.02 and 1.05, respectively. Thus in the present study, it is found that the biological activity of these complexes has a positive correlation with the lipophilicity. Previous studies have shown that the extent to which a complex penetrates a lipid bilayer usually increases with the lipophilicity of the side chains in the NHC ligands.[43,44] Table 4 summarizes the log *P* results.

TABLE 3 Intramolecular interactions of complex **5**

D–H···A	*d*(D–H) (Å)	d(H···A) (Å)	*d*(D···A) (Å)	>(DHA) (°)
C8–H8A···F3	0.99	2.360	3.323(3)	164
C8–H8A···F2	0.99	2.520	3.200(3)	125
C15–H15B···F1	0.99	2.530	3.204(3)	125
C21–H21A···N2	0.95	2.520	2.862(4)	101

3.6 | DNA binding

Absorption spectroscopy provided inceptive evidence of possible intercalation interactions between *Aa*-DNA and the Ag (I)–NHC complexes. In addition, viscosity measurements and fluorescence titration experiments were also performed in order to further evaluate the nature of DNA interaction with the complexes. A complex binding to DNA through intercalation usually results in hypochromism and bathochromism, as a result of the intercalative mode involving a strong stacking interaction between the planar aromatic chromophore and the intercalating agents.[45,46] The DNA binding properties of compounds **5**–**8** with *Aa*-DNA were investigated by UV–visible spectra in phosphate buffer (10 mM, pH = 7.4) containing 50 mM NaCl at 25 °C. As illustrated in Figure 4 and Table 5, with increasing concentration of *Aa*-DNA, the absorption intensities of these compounds are reduced by a large hypochromicity of 22 and 27% and smaller hypochromicity of 16 and 19%. There is no bathochromic shift in the observed spectra and the maximum absorption shows obvious hypsochromic adsorption (4.0–12.5.0 nm). The hypsochromic adsorption (blue shift) suggests that the compounds or a segment of the compound framework would fit into the base pairs of DNA as DNA–intercalating agents. Based on the decrease in absorbance and the hypsochromism observed, an intercalative binding mode is assigned to these complexes.

The intrinsic equilibrium binding constants of compounds **5**–**8** with *Aa*-DNA were calculated to be 3.367×10^6, 6.982×10^5, 8.376×10^5 and 1.223×10^6, respectively. The binding site size, *s*, obtained from absorbance titrations, is consistently between 0.81 and 1.05

TABLE 4 Lipophilicity (log *P*) for Ag(I)–NHC complexes **5**–**8**[a]

Complex	C_w ($\times 10^{-4}$ mol l^{-1})	C_o ($\times 10^{-4}$ mol l^{-1})	log *P*
5	1.0449	10.9705	1.02
6	0.9520	9.7662	1.05
7	0.2126	12.8260	1.78
8	0.1206	14.3857	2.06

[a]Log $P_{oct/wat}$ = log $[(C_o \times 10^{-4}\ M)/(C_w \times 10^{-4}\ M)]$, where C_w and C_o correspond to the concentration of complex in water and octanol, respectively.

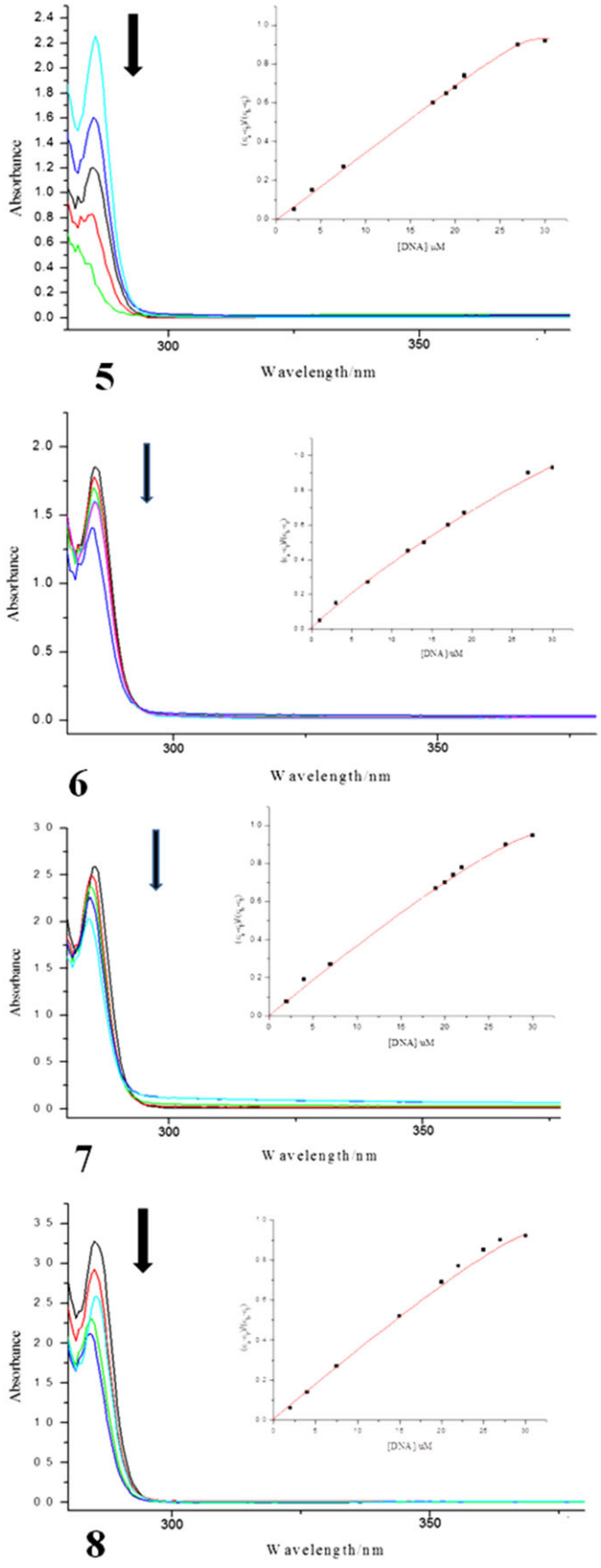

FIGURE 4 Absorption titration of complexes **5**–**8** with increasing amounts of *Aa*-DNA under conditions listed in Table 5. For each Ag–NHC complex, the spectral series show a progression of decreasing intensity with increasing [DNA]/[Ag]. The insets show plots of $(\varepsilon_a-\varepsilon_b)/(\varepsilon_a-\varepsilon_f)$ versus [DNA]μM, obtained from absorption spectral titration of the complexes

TABLE 5 DNA binding constants for Ag–NHC complexes **5**–**8**[a]

Complex	Hypsochromic shift (nm)	K_b[b]	s[b]	%H[c]
5	12.5(277)	3.367×10^6	1.05	27
6	4.0(273)	6.982×10^5	0.81	16
7	7.0(284)	8.376×10^5	0.84	19
8	9.0(285)	1.223×10^6	0.96	22

[a]Conditions: 10 mM phosphate, pH = 7.4, 50 mM NaCl, **5**–**8**.

[b]Errors in K_b and s values from absorption titrations are $\pm 0.6 \times 10^6$ and ±0.05. K_b is the DNA binding constant and s is the binding site size.

[c]Percent hypochromicity at specified wavelength in the absorption spectrum. The percentage hypochromicity was calculated using:[18] $\%H = (A_a - A_b/A_a) \times 100$, where A_a is the absorbance (free metal complex) and A_b is the absorbance at 260 nm (mixture of metal complex bound to DNA).

corresponding to a binding stoichiometry of about one Ag–NHC complex per base pair site. The values of K_b and site sizes were obtained from the spectroscopy emission data and these data were fitted to the equation previously derived.[23] The K_b values show that compound **5** with an extended aromatic side chain has the highest binding constant and consequently manifests the strongest binding properties with *Aa*-DNA compared to the other compounds possessing aliphatic side chains. This difference in the binding capacity may be due to the presence of an extended aromatic moiety in compound **5**, resulting in larger binding affinities of the complex compared to those of the others. In general the mode of action involves a strong stacking interaction between the planar aromatic chromophore and the intercalating agents.[45] Furthermore the K_b values and the binding strengths of the complexes follow the order **6** < **7** < **8** and this observation also correlates well with the lipophilic studies of the reported complexes. Therefore the result suggests that the length of the chain is valuable for DNA binding. Values of K_b obtained from absorption and fluorescence titrations in the present work are in reasonable agreement with those obtained from DNA titrations of similar complexes in the literature.[47–49] Also the K_b values of the benzimidazolium salts are sufficiently less than those of the corresponding Ag complexes available in the literature.[47–49]

3.7 | Fluorescence titration

To further study the binding capacity of the Ag–NHC complexes, fluorescence titrations were conducted (Figure 5 and Table 6). The fluorescence properties were determined to investigate the interactions between compounds **5**–**8** and *Aa*-DNA in phosphate buffer (10 mM phosphate, pH = 7.4, 50 mM NaCl). As depicted in Figure 5, the compounds show similar binding properties with *Aa*-DNA, exhibiting similar double emission bands in the region 310–325 nm corresponding to intraligand π*–π and π*–n transitions in the fluorescence spectra. The fluorescence intensities decrease markedly with increasing concentration of *Aa*-DNA. The quenching behaviours of *Aa*-DNA on the fluorescence of **5**–**8** are found to follow a conventional Stern–Volmer

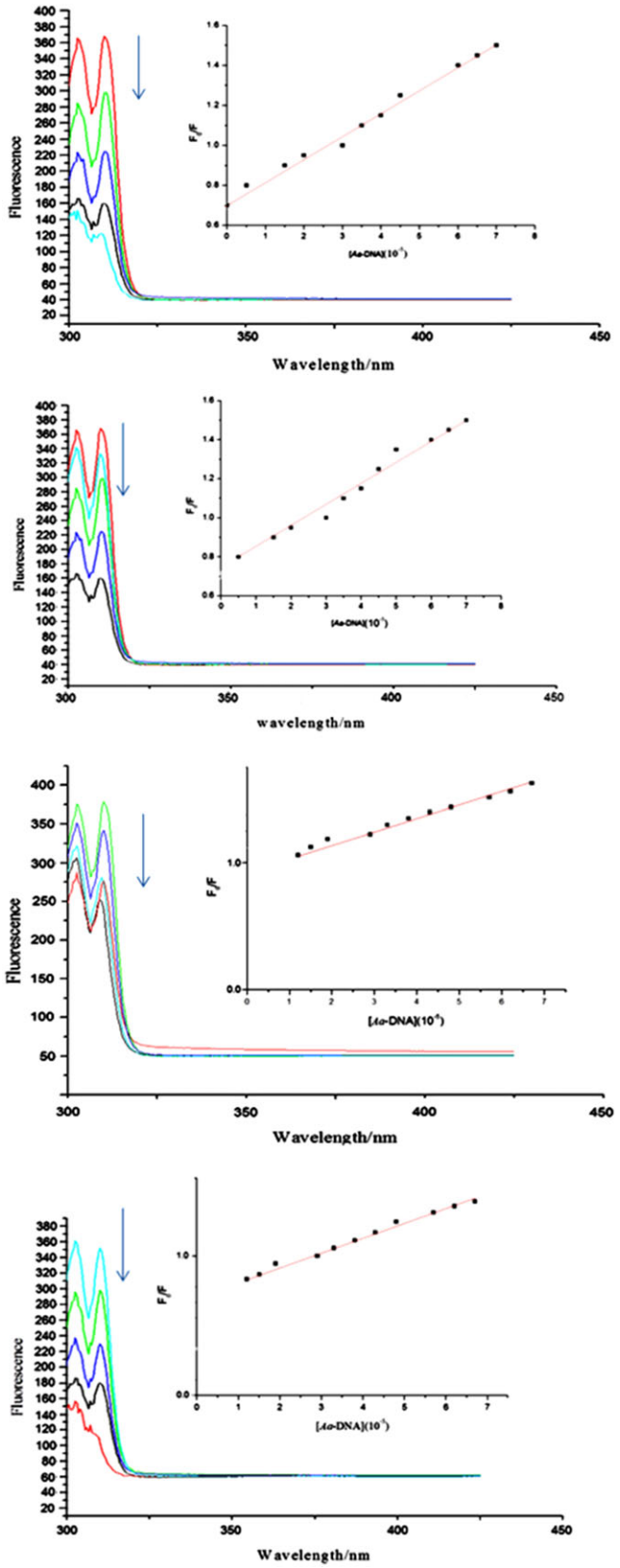

FIGURE 5 Fluorescence spectral changes of **5**–**8** upon addition of *Aa*-DNA (0–200 μl) in phosphate buffer (pH = 7.4) containing 50 mM NaCl and 2% DMSO at 25 °C. Insets: Stern–Volmer plots for the observed fluorescence enhancement upon addition of *Aa*-DNA to the Ag–NHC complexes [F_0/F] versus *Aa*-DNA(10^4)/M

TABLE 6 Fluorescence titration data for Ag–NHC complexes **5**–**8**[a]

Complex	K_b[b]	s[b]	F_0/F[c]
n	1.796×10^7	1.72	66
6	9.670×10^5	0.95	17
7	1.136×10^6	1.10	25
8	7.377×10^6	1.55	38

[a]Conditions: 10 mM phosphate, pH = 7.4, 50 mM NaCl, **5**–**8**.

[b]Errors in K_b and s values from fluorescence titrations are $\pm 0.21 \times 10^6$ and ±0.2.

[c]Ratio of fluorescence intensity of (Ag–NHC complex + *Aa*-DNA) to fluorescence intensity of Ag–NHC complex in buffer.

relationship.[50,51] The equations reveal that F_0/F increases in direct proportion to the increasing concentration of *Aa*-DNA, and the quenching constant K_{SV} defines the quenching efficiency of *Aa*-DNA. We have used the spectroscopic method to obtain values of equilibrium binding constants and examples of the florescence emission data are shown in Figure 5. Values of K_b and site size, s, were extracted from the data by fitting the data to the equations[23] with the modification that fluorescence intensity F replaces the ε values used for the absorption titrations. The fitting results from titrations of the Ag–NHC complexes are listed in Table 6.

The fluorescence intensities were quantified by plotting F_0/F as a function of *Aa*-DNA concentration, where F_0 and F are the fluorescence intensity without and with *Aa*-DNA. Stern–Volmer analysis gives a profound insight into the binding efficiency in terms of fluorescence enhancement of the complexes with increasing concentration of *Aa*-DNA. The calculated binding efficiencies are 1.796×10^7, 9.670×10^5, 1.136×10^6 and 7.377×10^6 for compounds **5**, **6**, **7** and **8**, respectively. The magnitude of K_b values obtained from the fluorescence titrations agree well with the order of magnitude for the absorption titrations (**6** < **7** < **8** < **5**); however, the results of fluorescence titrations have a larger range.

The quenching constant (*K*sv) values of the quencher are given by the ratio of intercept to slope, which defines the quenching efficiency of *Aa*-DNA and consequently the binding properties of the complexes. As shown by the Stern–Volmer plots in Figure 5 (insets), the *K*sv values are 0.3×10^5, 0.1×10^5, 0.12×10^5 and 0.25×10^5 M^{-1} for **5**, **6**, **7** and **8**, respectively. The Stern–Volmer plots indicate that the fluorescence of compound **5** linked by the aromatic side chain is more sensitive to the *Aa*-DNA concentrations than those of the others. These results are consistent with the observations as regards the absorption titrations and viscosity measurements in all items in this work. This result shows that all the complexes interact with *Aa*-DNA which provides further evidence that the metal complexes bind to *Aa*-DNA.

3.8 | DNA binding activity using viscometry

Viscosity measurement is used to study the changes in the viscosity of solutions due to DNA intercalation. This method

is also vital for discovering the nature of the binding of metal complexes to DNA.[52] An optimum intercalative mode usually causes a significant increase in the viscosity of DNA solution by pushing the base pairs apart and hence causing complete lengthening of the DNA helix. On the other hand, an incomplete intercalation of the ligand may also bend the helix and as a result reduce its effective length and consequently reduce the DNA viscosity.[3] Therefore an increase in solution viscosity is a reflection of molecules intercalating into DNA.[54]

In order to further probe the binding nature of the complexes to *Aa*-DNA, the viscosity of solutions of complexes with *Aa*-DNA was measured. The result of the viscosity titration plots is shown in Figure 6. The viscosity of *Aa*-DNA is increased with an increase of the concentration of the test compounds, using ethidium bromide as the positive control[55] and DMSO as the negative control. In the solvent control test, the effect of 10% DMSO on the viscosity was studied, and it is shown to be a non-intercalator. Positive slopes are observed for all the complexes, although with values less than that of ethidium bromide, whereas the known non-intercalator DMSO produces a zero slope line. Based on the foregoing, the result has also established a considerable intercalating mode of the interactions of these complexes.[56]

3.9 | Nuclease activity of benzimidazolium salts and Ag (I)–NHC complexes

3.9.1 | Deoxyribonuclease (DNase) activity of test compounds

The DNase activity of the test compounds at varying concentrations and incubation periods were analysed on agarose gel s using plasmid DNA. Incubation of plasmid DNA with the test salts to evaluate their DNase activities reveals a concentration-dependent activity pattern (Figures 7 and 8). DNA degradation (salts **2**–**4**) and cleavage (nicked circular form; salt **1**) are observed after an incubation period of 24 h with 200 μg ml^{-1} of the test ligands (Figure 7A). At the lower concentration of 100 μg ml^{-1}, DNA degradation and cleavage

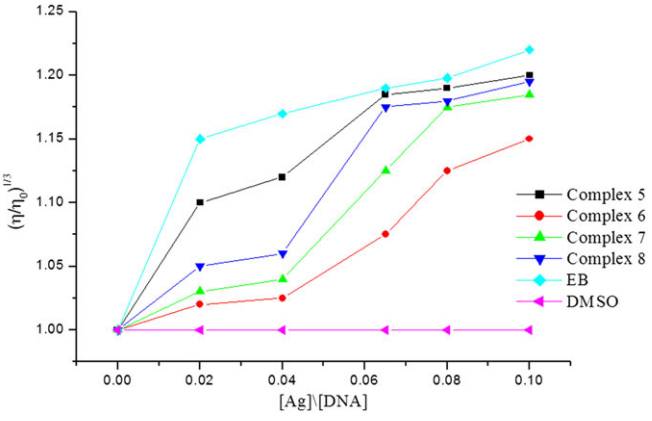

FIGURE 6 Viscosity titration of *Aa*-DNA and each of the four Ag–NHC complexes, negative control (DMSO) and positive control (ethidium bromide, EB). Conditions: 10 mM phosphate buffer, pH = 7, 50 mM NaCl, [Ag] = 25 μM

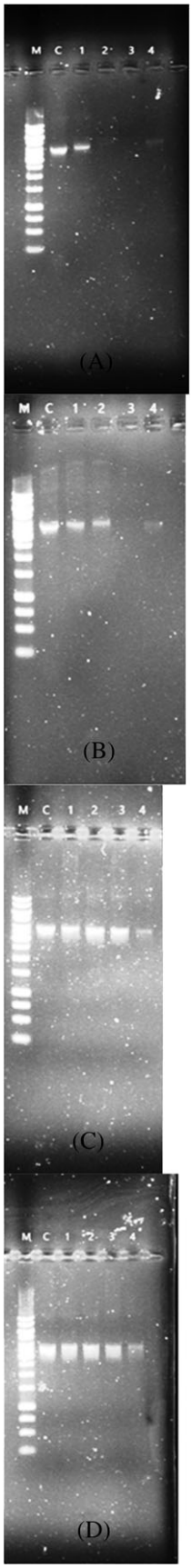

FIGURE 7 Deoxyribonuclease activity assay on plasmid DNA after a 24 h incubation period using (A) 200, (B) 100, (C) 50 and (D) 25 μg ml^{-1} of the test salts. M: 1 kb molecular marker (Fermentas); C: control plasmid DNA; 1: plasmid DNA + **1**; 2: plasmid DNA + **2**; 3: plasmid DNA + **3**; 4: plasmid DNA + **4**

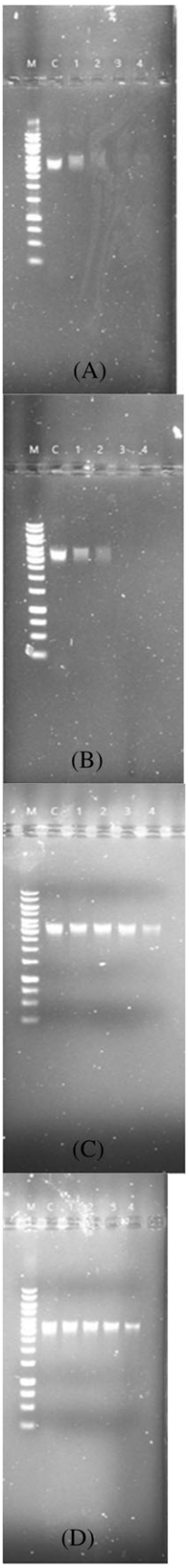

FIGURE 8 Deoxyribonuclease activity assay on plasmid DNA after an 8 h incubation period using (A) 200, (B) 100, (C) 50 and (D) 25 μg ml^{-1} of the test salts. M: 1 kb molecular marker (Fermentas); C: control plasmid DNA; 1: plasmid DNA + **1**; 2: plasmid DNA + **2**; 3: plasmid DNA + **3**; 4: plasmid DNA + **4**

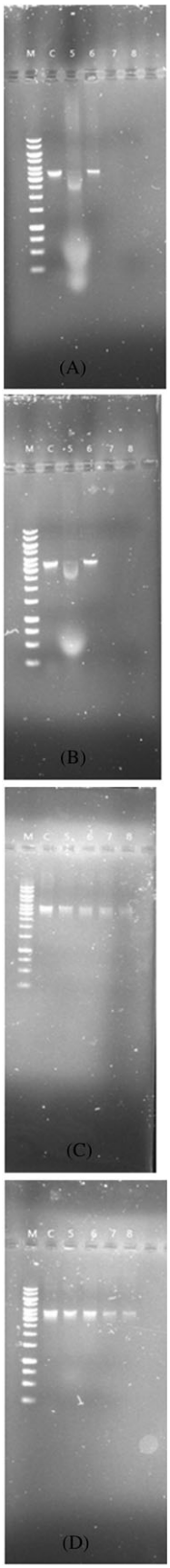

FIGURE 9 Deoxyribonuclease activity assay on plasmid DNA after a 24 h incubation period using (A) 200, (B) 100, (C) 50 and (D) 25 μg ml^{-1} of the test complexes. M: 1 kb molecular marker (Fermentas); C: control plasmid DNA; 5: plasmid DNA + **5**; 6: plasmid DNA + **6**; 7: plasmid DNA + **7**; 8: plasmid DNA + **8**

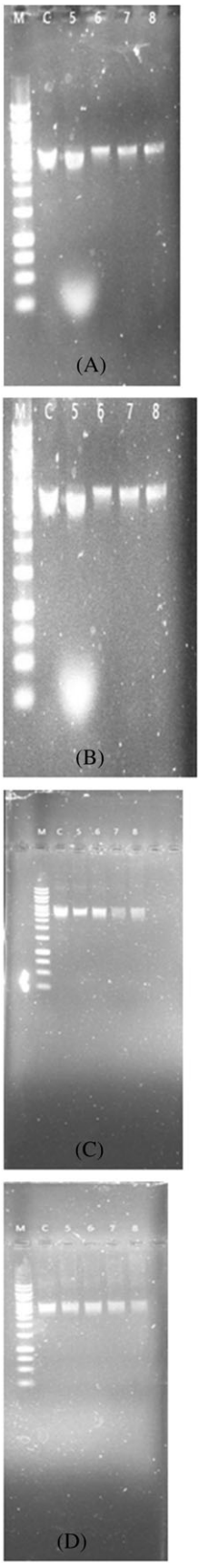

FIGURE 10 Deoxyribonuclease activity assay on plasmid DNA after an 8 h incubation period using (A) 200, (B) 100, (C) 50 and (D) 25 μg ml^{-1} of the test complexes. M: 1 kb molecular marker (Fermentas); C: control plasmid DNA; 5: plasmid DNA + **5**; 6: plasmid DNA + **6**; 7: plasmid DNA + **7**; 8: plasmid DNA + **8**

are observed (Figure 7B). However, salt **3**, which hitherto nearly completely degraded the DNA at a concentration of 200 μg ml^{-1} (Figure 7A), only cleaves it at 100 μg ml^{-1} (Figure 7B). Lower DNase activities are observed when using lower concentrations of the test salts (Figure 7C, D).

At 8 h of incubation, the test ligands induce varying DNase activity levels based on the concentration of the salts (Figure 8). Pronounced degradation of DNA is observed when using salts **3** and **4** at both 100 and 200 μg ml^{-1} (Figure 8A, B) compared to concentrations of 25 and 50 μg ml^{-1} (Figure 8C, D). Cleavage abilities were however displayed by the salts at the lower concentrations of 25 and 50 μg ml^{-1} (Figure 8C, D).

Figure 9 shows the DNase activities of different concentrations of the complexes after a 24 h incubation period. Higher concentrations (100 and 200 μg ml^{-1}) of complexes **7** and **8** completely degrade the plasmid DNA, while partial degradation and cleavage are observed for complexes **5** and **6**, respectively. None of the complexes completely degrades the plasmid DNA at lower concentrations (50 and 25 μg ml^{-1}), although degradation/cleavage is observed for complexes **7** and **8**.

Incubating the complexes for a shorter period (8 h) leads to higher concentrations of complexes **6–8** inducing cleavage (nicked circular DNA) of the plasmid DNA (Figure 10). Nearly similar cleavage abilities are displayed by complexes **6–8** at concentrations of 100 and 200 μg ml^{-1} (Figure 10A, B). DNase activities at lower concentrations are minimal compared 1to higher concentrations. However, even at lower concentrations, complexes **7** and **8** exhibit higher DNase activities compared to complexes **5** and **6** as observed in the conspicuous decrease in intensity of the DNA band (Figure 10C, D).

The nature of reactive intermediates involved in DNA cleavage by the complexes is not clear. However, the contribution of an oxidative cleavage mechanism can be invalidated, and it may be said that, in the present study, cleavage most probably occurs primarily through hydrolytic pathways.

4 | CONCLUSIONS

A series of four new symmetrically substituted benzimidazolium salts and their Ag(I)–NHC complexes were synthesized and characterized using various spectral and analytical techniques. All reported compounds were stable to air and moisture and their stability in the biological medium was investigated and found to be acceptable for the studies. Molecular structure of complex **5** was established using single-crystal X-ray diffraction. All the complexes in this study showed moderate to significant DNA cleavage/degradation activity in the absence of oxidizing agent. Incubation of plasmid DNA with the test compounds to evaluate their DNase activities revealed a time- and concentration-dependent activity pattern. Additionally, UV–visible absorption spectral,

emission spectral and viscosity measurement studies revealed the intercalative mode of binding of theses complexes with DNA, showing considerable intrinsic binding constants. DNA binding assay showed that complex **5** can strongly interact with DNA and has a better DNA binding ability than the other complexes. DNA binding properties suggested that the length of the linker is of benefit for improving the DNA binding capacity of these compounds. The lipophilicity assay indicates that the activity of the Ag(I)–NHC complexes correlates well with the lipophilicity of the complexes. Further work is ongoing on the *in vivo* activity of the newly designed complexes against all stages of the major dengue vector *A. albopictus*, the results of which will be reported in due course.

ACKNOWLEDGMENTS

R. A. Haque and M. R. Razali thank Universiti Sains Malaysia for the Research University grant 1001/PKIMIA/811346. P. O. Asekunowo thanks USM for a postdoctoral fellowship.

REFERENCES

[1] B. J. Pages, D. L. Ang, E. P. Wright, J. R. Aldrich-Wright, *Dalton Trans.* **2015**, *44*, 3505.

[2] P. O. Asekunowo, R. A. Haque, *J. Coord. Chem.* **2014**, *67*, 3649.

[3] P. O. Asekunowo, R. A. Haque, M. R. Razali, S. Budagumpi, *Appl. Organomet. Chem.* **2015a**, *29*, 126.

[4] P. O. Asekunowo, R. A. Haque, M. R. Razali, *Transition Met. Chem.* **2015b**, *40*, 79.

[5] A. C. Komor, J. K. Barton, *Chem. Commun.* **2013**, *49*, 3617.

[6] S. J. Lippard, *Acc. Chem. Res.* **1978**, *11*, 211.

[7] B. Nordén, P. Lincoln, B. Akerman, E. Tuite, *Met. Ions Biol. Syst.* **1996**, *33*, 177.

[8] A. R. Beaudoin, *Neurotoxicol. Teratol.* **1973**, *7*, 65.

[9] J. H. Looker, L. W. Wilson Jr., *J. Heterocycl. Chem.* **1965**, *2*, 348.

[10] O. Kennard, *Pure Appl. Chem.* **1993**, *65*, 1213.

[11] J. M. T. Hamilton-Miller, S. Shah, *Int. J. Antimicrob. Agents* **1996**, *7*, 97.

[12] S. Bassetti, J. Hu, R. B. Agostino, R. J. Sherertz, *Antimicrob. Agents Chemother.* **2001**, *45*, 1535.

[13] R. Palchaudhuri, P. J. Hergenrother, *Curr. Opin. Biotechnol.* **2007**, *18*, 497.

[14] World Health Organization, Dengue and severe dengue, Fact sheet no. 117, **May 2015**.

[15] S. W. Avicor, M. F. Wajidi, F. M. El-garj, Z. Jaal, Z. S. Yahaya, *Protein J.* **2014**, *33*, 457.

[16] J. Vontas, E. Kioulos, N. Pavlidi, E. Morou, A. della Torre, H. Ranson, *Pestic. Biochem. Physiol.* **2012**, *104*, 126.

[17] *Apex II*, Bruker AXS Ltd, Madison, WI **2005**.

[18] G. M. Sheldrick, *Acta Crystallogr. A* **2008**, *64*, 112.

[19] L. J. Barbour, *J. Supramol. Chem.* **2001**, *1*, 189.

[20] A. J. Leo, *Chem. Rev.* **1993**, *93*, 1281.

[21] F. M. A. El-garj, S. W. Avicor, M. F. F. Wajidi, Z. Jaal, *Asian Biomed.* **2015**, *9*, 313.

[22] M. E. Reichnann, S. A. Rice, C. A. Thomas, P. Doty, *J. Am. Chem. Soc.* **1954**, *76*, 3047.

[23] M. T. Carter Rodriguez, A. J. Bard, *J. Am. Chem. Soc.* **1989**, *111*, 8901.

[24] J. R. Lakowicz, G. Webber, *Biochemistry* **1973**, *12*, 4161.

[25] X. W. Liao, W. J. Pan, R. W. He, H. W. Guo, P. Ying, J. Z. Lu, *Chem. Biol. Drug Des.* **2014**, *83*, 367.

[26] J. Z. Lu, H. W. Guo, X. D. Zeng, Y. L. Zhang, P. Zhao, J. Jiang, L. Q. Zang, *J. Inorg. Biochem.* **2012**, *112*, 39.

[27] R. Kishore, S. K. Das, *J. Mol. Struct.* **2013**, *1053*, 38.

[28] H. M. J. Wang, C. Y. L. Chen, I. J. B. Lin, *Organometallics* **1999**, *18*, 1216.

[29] S. Demir, I. Özdemir, B. Çetinkaya, H. Arslan, D. VanDerveer, *Polyhedron* **2011**, *30*, 195.

[30] N. A. Piro, J. S. Owen, J. E. Bercaw, *Polyhedron* **2004**, *23*, 2797.

[31] W. Wang, F. Wang, M. Shi, *Organometallics* **2010**, *29*, 928.

[32] M. V. Baker, D. H. Brown, V. J. Hesler, B. W. Skelton, A. H. White, *Organometallics* **2007**, *26*, 250.

[33] S. Budagumpi, R. A. Haque, A. W. Saalman, M. Z. Ghdhayeb, *Inorg. Chim. Acta* **2012**, *394*, 61.

[34] X. Hu, Y. Tang, P. Gantzel, K. Meyer, *Organometallics* **2003**, *22*, 612.

[35] H. M. Lee, P. L. Chiu, C. H. Hu, C. L. Lai, Y. C. Chou, *J. Organomet. Chem.* **2005**, *690*, 403.

[36] D. J. Nielsen, K. J. Cavell, B. W. Skelton, A. H. White, *Inorg. Chim. Acta* **2003**, *352*, 143.

[37] J. Pytkowicz, S. Roland, P. Mangeney, *J. Organomet. Chem.* **2001**, *631*, 157.

[38] S. B. Kalia, K. Lumba, G. Kaushal, M. Sharma, *Indian J. Chem.* **2007**, *46*, 1233.

[39] W. J. Geary, *Coord. Chem. Rev.* **1971**, *7*, 81.

[40] P. De Fremont, N. Marion, S. P. Nolan, *Coord. Chem. Rev.* **2009**, *253*, 862.

[41] W. A. Herrmann, T. Weskamp, V. P. Boehm, *Adv. Organometal. Chem.* **2002**, *48*, 1.

[42] M. P. Edward, D. A. Price, *Annu. Rep. Prog. Chem.* **2010**, *45*, 381.

[43] M. V. Baker, P. J. Barnard, S. J. Berners-Price, S. K. Brayshaw, J. L. Hickey, B. W. Skelton, A. H. White, *Dalton Trans.* **2006**, *30*, 3708.

[44] L. Oehninger, M. Stefanopoulou, H. Alborzinia, J. Schur, S. Ludewig, K. Namikawa, I. Ott, *Dalton Trans.* **2003**, *42*, 1657.

[45] R. Breslow, I. E. Overman, *J. Am. Chem. Soc.* **1970**, *92*, 1075.

[46] P. F. Pasternack, F. J. Gibbs, J. Villatrnaca, *Biochemistry* **1983**, *22*, 2406.

[47] R. A. Haque, S. Budagumpi, S. Y. Choo, M. K. Choong, B. E. Lokesh, K. Sudesh, *Appl. Organomet. Chem.* **2012**, *26*, 689.

[48] O. Sánchez, S. González, Á. R. Higuera-Padilla, Y. León, D. Coll, M. Fernández, P. Taylor, I. Urdanibia, H. R. Rangel, J. T. Ortega, W. Castro, *Polyhedron* **2016**, *110*, 14.

[49] S. A. Tysoe, R. J. Morgan, A. D. Baker, T. C. Strekas, *J. Phys. Chem.* **1993**, *97*, 1707.

[50] Y. Z. Zhang, X. X. Chen, J. Dai, X. P. Zhang, *Luminescence* **2008**, *23*, 150.

[51] D. Zhao, W. H. Chan, Z. K. He, T. Qiu, *Anal. Chem.* **2009**, *81*, 3537.

[52] S. Satyanarayana, J. C. Dabrowiak, J. B. Chaires, *Biochemistry* **1992**, *31*, 9319.

[53] F. Arjmand, S. Parveen, M. Afzal, M. Shahid, *J. Photochem. Photobiol. B* **2012**, *114*, 15.

[54] D. Suh, J. B. Chaires, *Bioorg. Med. Chem.* **1995**, *3*, 723.

[55] H. M. Sobell, C. C. Tsai, S. C. Jain, S. G. Gilbert, *J. Mol. Biol.* **1977**, *114*, 333.

[56] A. Wolfe, G. H. Shimer, T. Meehan, *Biochemistry* **1987**, *26*, 6392.

SUPPORTING INFORMATION

Additional Supporting Information may be found online in the supporting information tab for this article.

How to cite this article: Asekunowo, P. O., Haque, R. A., Razali, M. R., Avicor, S. W., and Wajidi, M. F. F. (2016), Dose-, time-and lipophilicity-dependent silver(I)–N-heterocyclic carbene complexes: Synthesis, characterization and interaction with plasmid and Aedes albopictus DNA, *Appl Organometal Chem*, doi: 10.1002/aoc.3655